Support Information

ZIF-67/BiOCl nanocomposite for highly efficient detection of NO_2 gas at Room temperature

Jiahui Fan[a], Lin Jiang[a], He Lv[a], Fangjie Qin[a], Yihe Fan[a], Jue Wang[a], Muhammad Ikram[b, *], Keying Shi[a, *]

a. Key Laboratory of Functional Inorganic Material Chemistry, Ministry of Education. School of Chemistry and Material Science, Heilongjiang University, Harbin, 150080, P. R. China.

b. Zhengzhou Research Institute, Harbin Institute of Technology, Zhengzhou 450000, China.

c. School of Mechanical and Electronic Engineering, Qingdao Binhai University, Qingdao 266555, Shandong, P.R. China

* Corresponding author

Corresponding author: Tel: +86 451 86609141; +86 451 86604920

E-mail: ikram@hit.edu.cn

E-mail: shikeying2008@163.com

Fax: +86 4518667 3647; Tel: +86 451 8660 9141

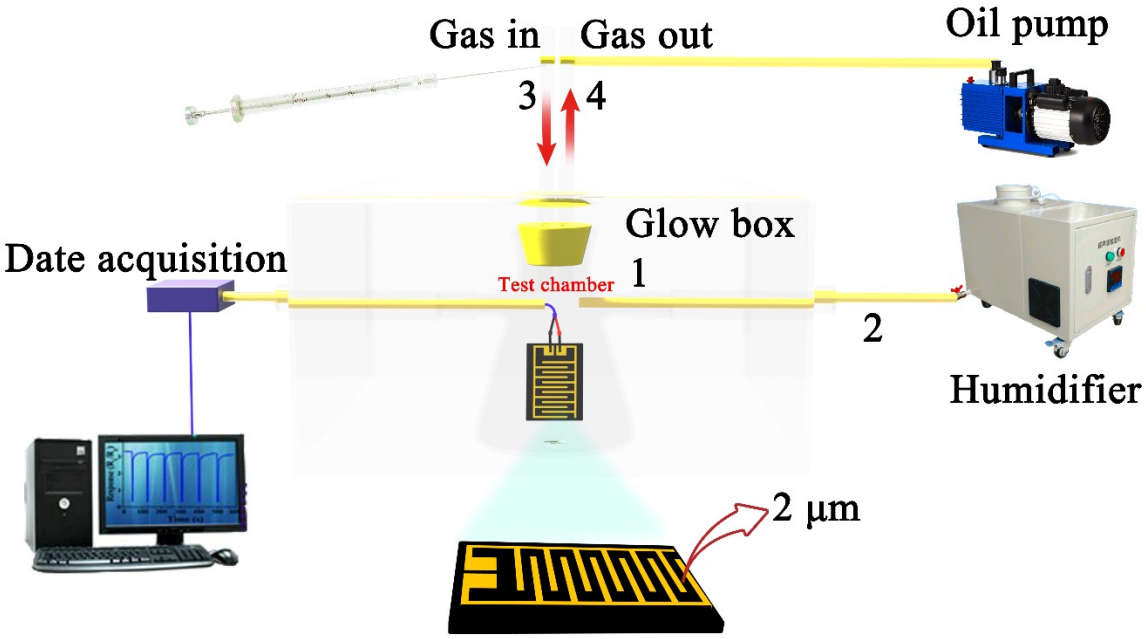

Scheme S1 Diagram of the sensing process for the gas transportation system.

Materials

All reagents are of analytical grade and have not been further purified. Bismuth nitrate pentahydrate ($Bi(NO_3)_3 \cdot 5H_2O$, 99%) was purchased from Sinopharm Chemical Reagent Co., Ltd. Cobalt nitrate hexahydrate ($Co(NO_3)_2 \cdot 6H_2O$, 99%) and Ethyne glycol (EG) were purchased from Xilong Chemical Co., Ltd. Methanol (CH_3OH) was purchased from Tianjin Fuyu Fine Chemical Co., Ltd. Anhydrous ethanol (C_2H_5OH) and Hexadecyltrimethylammonium bromide (CTAB) was purchased from Tianjin Comio Chemical Reagent Co., Ltd. 2-Methylimidazole and Poly(diene dimethyl ammonium chloride) solution (PDDA) were purchased from Shanghai Aladdin Biochemical Technology Co., Ltd.

Table S1. The comparison of present work on ZIF-67/BiOCl nanocomposite with the reported literatures.

Materials	Gas	W. T. (°C)	Gas Conc. (ppm)	T_{res}/T_{rec} (s)	Sensitivity (R_a/R_g)	LOD (ppm)	Ref
This Work	**NO_2**	**RT**	**100**	**7s/86**	**44.81②**	**0.05**	**This Work**
Co_3O_4/g-C_3N_4 (ZIF-67 drived)	NO_2	RT	100	1.06/26.6	17.83②	0.05	[1]
SnO_2/ZIF-8	NO_2	300	10	64/45	167②	0.15	[2]
ZIF-8/In_2O_3	NO_2	140	1	80/133	5.6②	0.01	[3]
Au/BiOCl	CO_x	200-300 ℃	100-400 pm	63.2%①	9s	-	[4]
BiOCl	CO	300-400 ℃	800 ppm	90%①	4.3s	-	[5]
BiOCl	Ethanol	180 ℃	1000 ppm	30%①	-	-	[6]
a-C /TeO_2	NO_2	50	10	--	1.978②	--	[7]
g-C_3N_4@TiO_2	NO_2	RT	100	329/372	19.7②	0.001	[8]
Cu-MoS_2	NO_2	100	20	54/82	30②	2	[9]
BP microribbons	NO_2	RT	100	--	66%①	0.4ppb	[10]
Cu_2O/CuO-0.5	NO_2	RT	10	23/159	82.0%①	0.01	[11]
WO_3/WS_2-300	NO_2	RT	50	29/489	455.3%①	~5 ppb	[12]

W.T.: Working temperature; LOD: limit of detection; RT: Room temperature.

①: S=|Ra–Rg|/Ra×100% or S=|Rg–Ra|/Ra×100%； ②: S=Ra/Rg

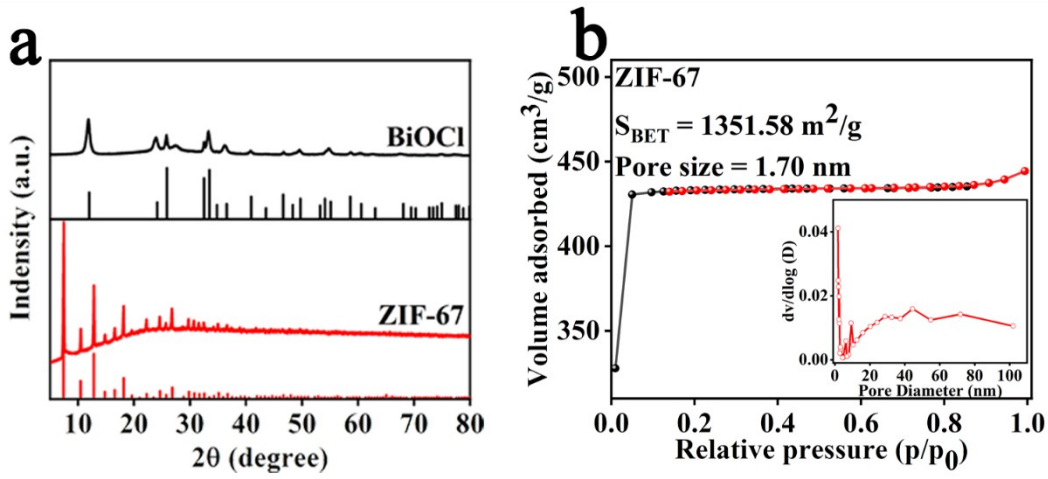

Fig. S1 (a) XRD pattern of the pristine BiOCl NSs and ZIF-67; (b) nitrogen adsorption and desorption isotherms of as-prepared ZIF-67 (Inset shows the aperture distribution).

Table S2 The textual characteristics of nitrogen adsorption and desorption isotherms of all ZBO.

Samples	S_{BET} (m^2/g)	Pore size (nm)
ZIF-67	1351.58	1.70
ZBO-1	1307.06	2.91
ZBO-2	1251.02	3.62
ZBO-3	1146.16	4.35

Table S3 Assignment of the Raman bands of ZIF-67,

Raman Bands cm^{-1}	Assignment	Ref
423	Co-N	
684	Imdz ring puckering, H oop bend	
738	C=N oop bend, δ N-H	
1121	C-H oop bend	
1144	ν C5-N	13
1178	ν C−N + N−H wag	
1303	ring expansion	
1382	δ CH_3	
1456	C-H	
1505	C_2N_3 + C_4N_3 + ν C_5N1 + N-H	

Imdz: imidazole

Oop: out of plane

Ar: aromatic

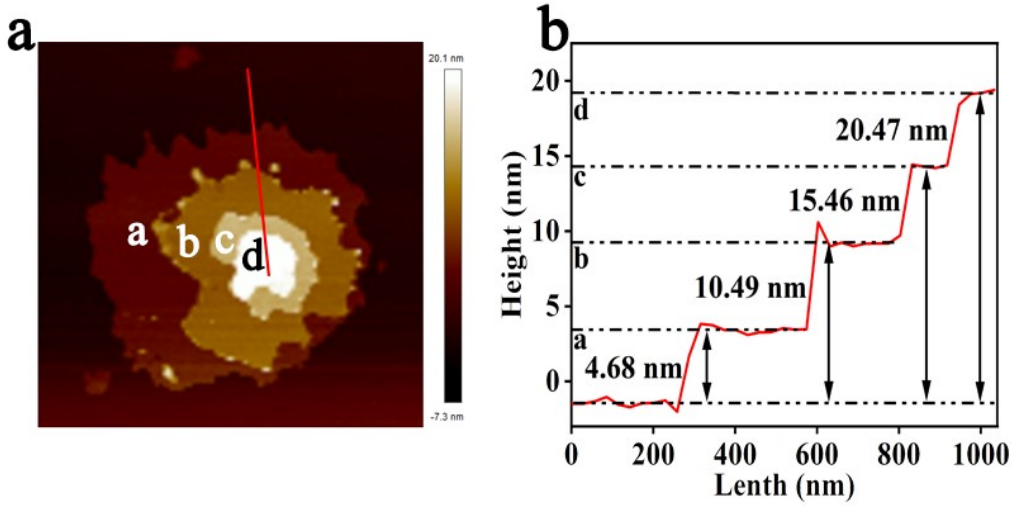

Fig. S2 (a) AFM image of BiOCl, with red lines indicating the different regional height profiles; (b) the height profile of the red line reflects the thickness of the BiOCl NSs.

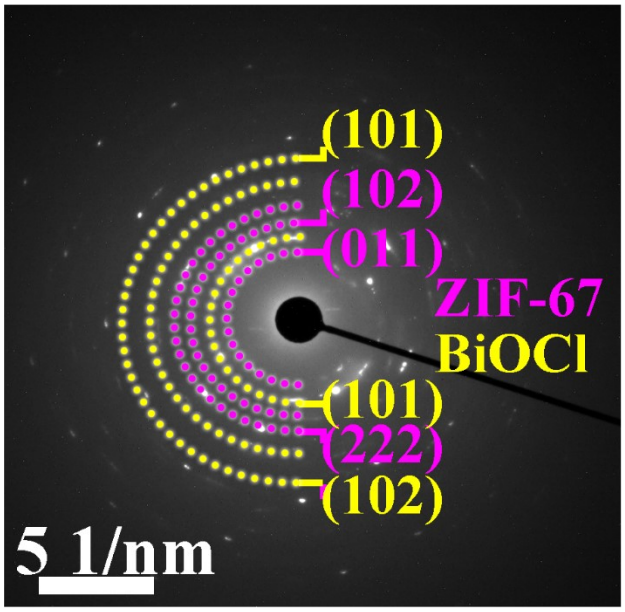

Fig. S3 Selected area electron diffraction (SAED) of ZBO-2

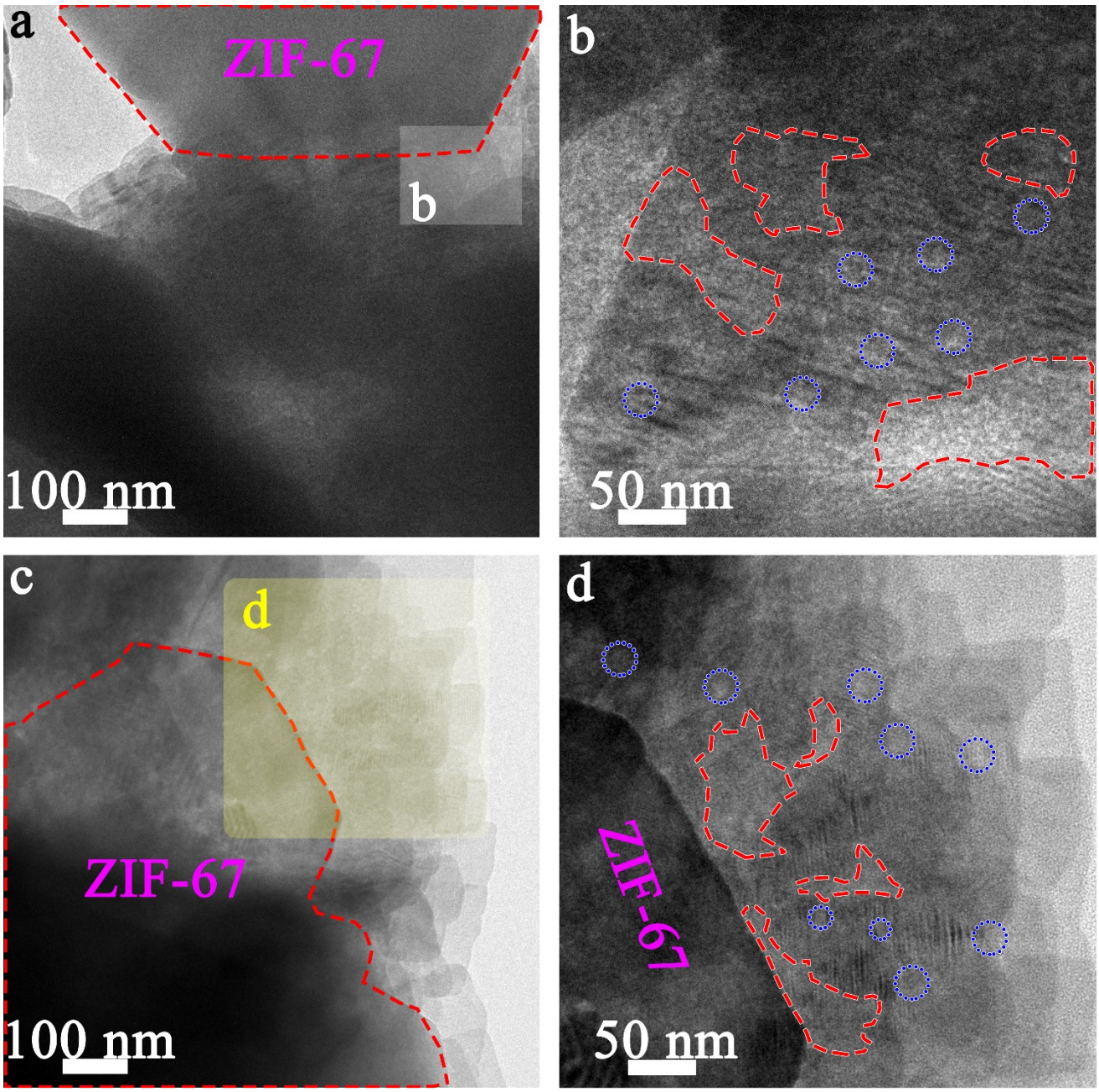

Fig. S4. (a-d) HRTEM images of ZBO-2 (red lines show surface defects in BiOCl NSs, blue lines indicate points defects).

Table S4. The XPS peak positions and peak area ratio (%) for Co

Sample	**ZBO-2**		**ZBO-2+NO_2**	
Peaks	**Co^{2+}**	**Co^{3+}**	**Co^{2+}**	**Co^{3+}**
Binding energy (eV)	785.4 801.5	797.1 781.5	785.5 802.7	797.7 781.8
Peak area ratio (%)	50.3	49.7	48.9	51.1
Peak area ratio (Co^{3+}/Co^{2+})	0.98		1.04	

Table S5 O1s peak position and peak area ratio (%) of ZBO-2 and ZBO-2+NO_2 samples O_l: lattice oxygen; O_V: oxygen vacancy; O_c: chemisorbed oxygen

Sample	**ZBO-2**			**ZBO-2+NO_2**		
Peak	**O_l**	**O_V**	**O_C**	**O_l**	**O_V**	**O_C**
Binding energy (eV)	535.3	532.9	531.7	535.9	533.4	532.6
Peak area ratio (%)	35.9	43.6	20.5	34.4	39.7	25.9

Raw materials	R_1 (Ω)	C_1 (F)	R_2 (Ω)	C_2 (F)
ZBO-1	4.417×10^{5}	1.207×10^{-12}	1.268×10^{6}	1.261×10^{-10}
ZBO-2	4.463×10^{4}	7.015×10^{-11}	1.081×10^{6}	3.691×10^{-11}
ZBO-3	5.170×10^{4}	7.088×10^{-11}	1.207×10^{6}	3.746×10^{-11}
BiOCl	5.692×10^{7}	8.305×10^{-12}	8.377×10^{7}	5.347×10^{-10}

Table S6 Parameters obtained by fitting experimental curve to equivalent circuit (In-air atmosphere).

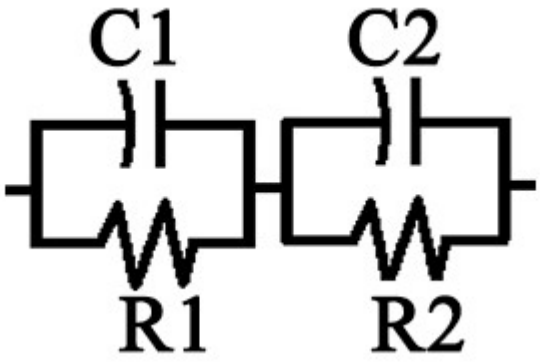

Fig. S5 The equivalent circuit model used to interpret the EIS data.

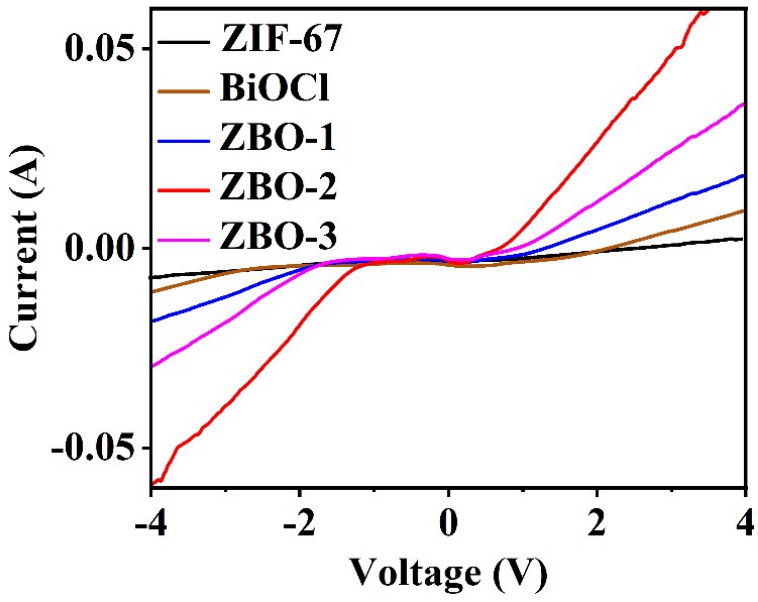

Fig. S6 Current-Voltage (I-V) behavior measured at RT in air.

Table S7 Response, response time and recovery time of **ZBO** sensors at room temperature (RT=25 ℃, RH 25%).

Sample	**ZBO-1**			**ZBO-2**			**ZBO-3**			**BiCOl**		
NO_2(ppm)	**S**	**T/s**	**Tr/s**	**S**	**T/s**	**Tr/s**	**S**	**T/s**	**Tr/s**	**S**	**T/s**	**Tr/s**
100	40.32	7.98	41.34	44.81	7.00	44.00	42.56	7.58	43.33	20.54	7.47	66.98
50	30.67	14.65	31.30	38.53	10.00	18.18	35.34	14.35	32.66	6.06	18.07	56.88
30	19.28	18.66	58.67	24.73	13.58	17.00	22.41	17.38	30.91	3.14	24.25	50.25
10	15.33	20.00	20.50	18.76	15.82	17.00	17.73	18.48	29.37	1.78	27.01	45.60
5	9.25	23.70	15.80	10.47	16.00	9.00	9.64	22.00	27.49	1.59	29.87	35.08
3	4.31	27.59	19.60	5.30	18.83	8.36	5.20	24.58	24.45	1.44	32.40	30.55
1	1.88	28.37	12.50	1.95	20.00	7.18	1.90	26.98	21.26	1.27	38.47	20.02
0.5	1.54	33.75	10.50	1.63	22.48	6.70	1.42	29.67	15.59			
0.3	1.21	34.66	8.50	1.40	25.96	5.24	1.26	32.58	10.40			
0.1	1.01	38.95	6.40	1.21	26.85	4.35	1.18	35.67	8.30			
0.05	0.98	42.65	3.10	1.11	28.65	2.50	23.51	16.00	85.00			

*S: Response T_s: Response time T_r: Recovery time

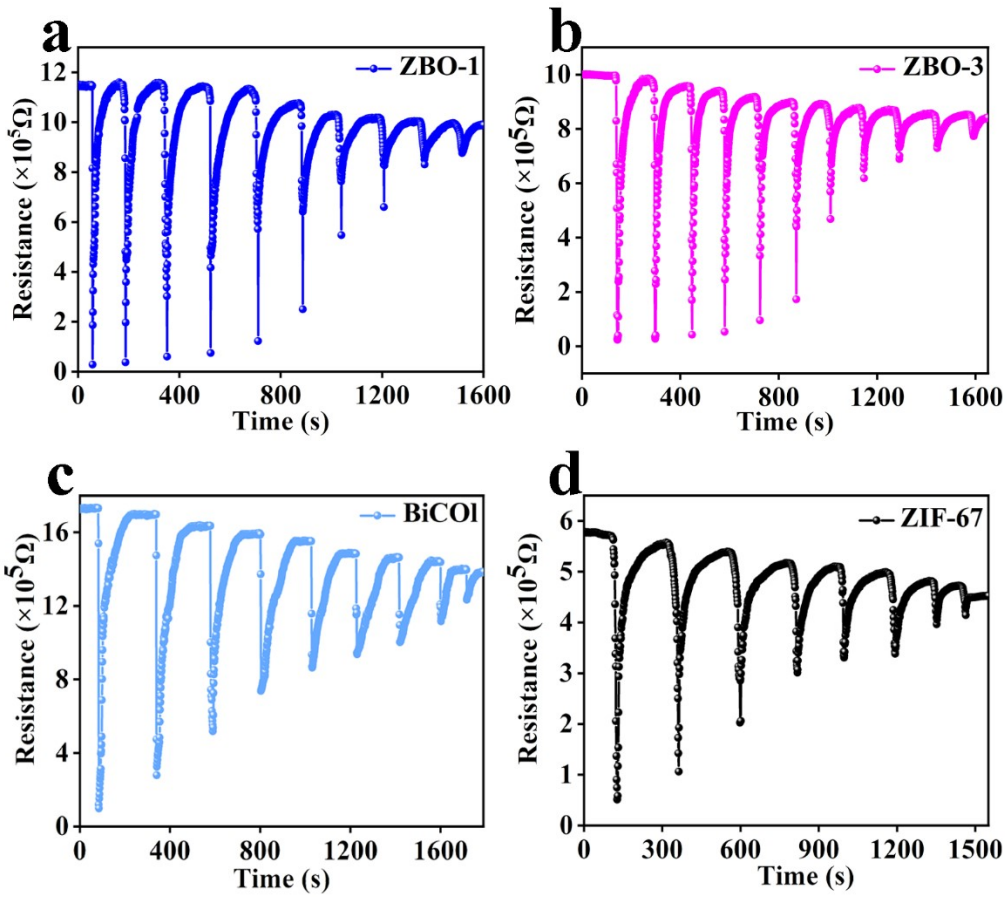

Fig. S7 Dynamic response-recovery curves of (a) ZBO-3; (b) ZBO-1; (c) BiOCl; (d) ZIF-67

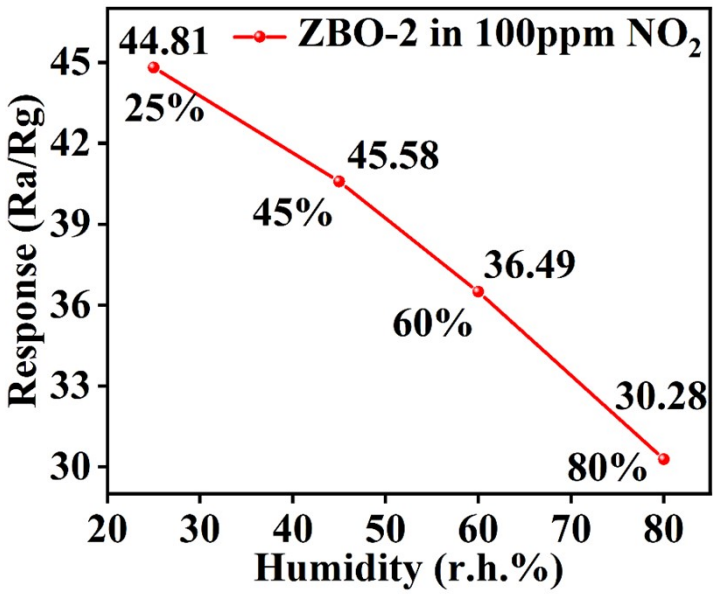

Fig. S8 Response value of ZBO -2 sensor at different humidity conditions.

Calculation for limit of detection (LOD):

The noise of the sensor is calculated using the change in the relative response of the sensor over the baseline (root mean square deviation) [14-16]. According to Eq. (1) below, and Si and S obtained by polynomial fitting method in Figure 6a, [Vx]^2 can be collected. According to Eq. (2), the sensor noise is 0.00189, and according to Eq. (3), the theoretical detection limit (for a signal-to-noise ratio of 3) is about 10 ppb. Therefore, the theoretical detection limit of 10 ppb to NO_2 at RT.

$$Vx^2 = \Sigma(Si - S)^2 \quad (1)$$

$$rms = \sqrt{\frac{Vx^2}{N}} \quad (N = 50)$$

$$LOD = 3 * \left(\frac{rms}{slope}\right) \quad (3)$$

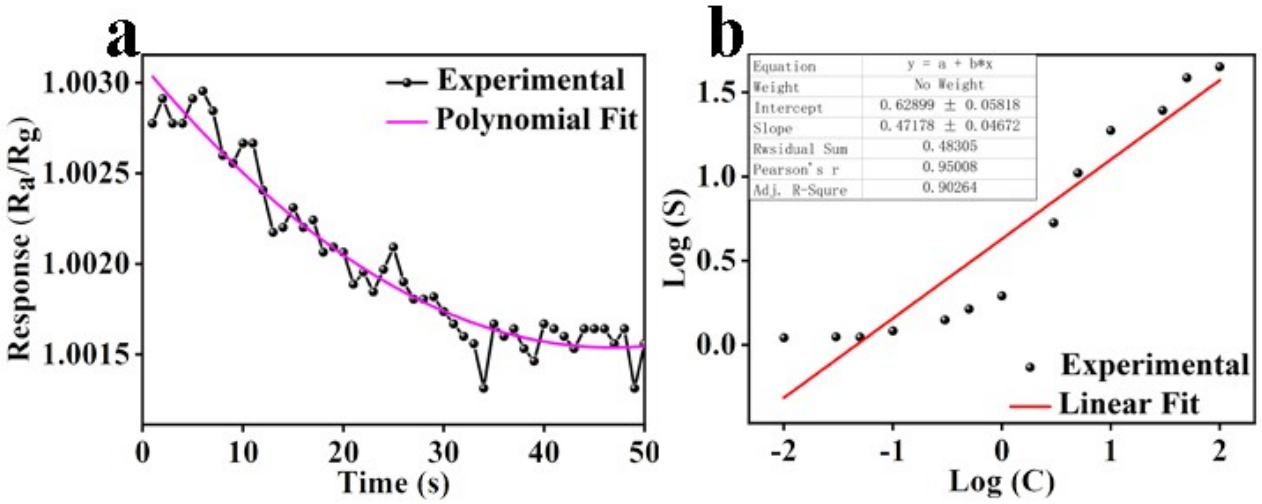

Fig. S9 (a) The curve obtained by fifth-order polynomial fitting the first 50 response points in the response-time baseline of the ZBO-2 sensor before the injection of NO_2. The response values before and after fitting are recorded as Yi and Y, respectively; (b) the curve with detailed data obtained by linear fitting the response points in the NO_2 sensing measurement of Figure 6a.

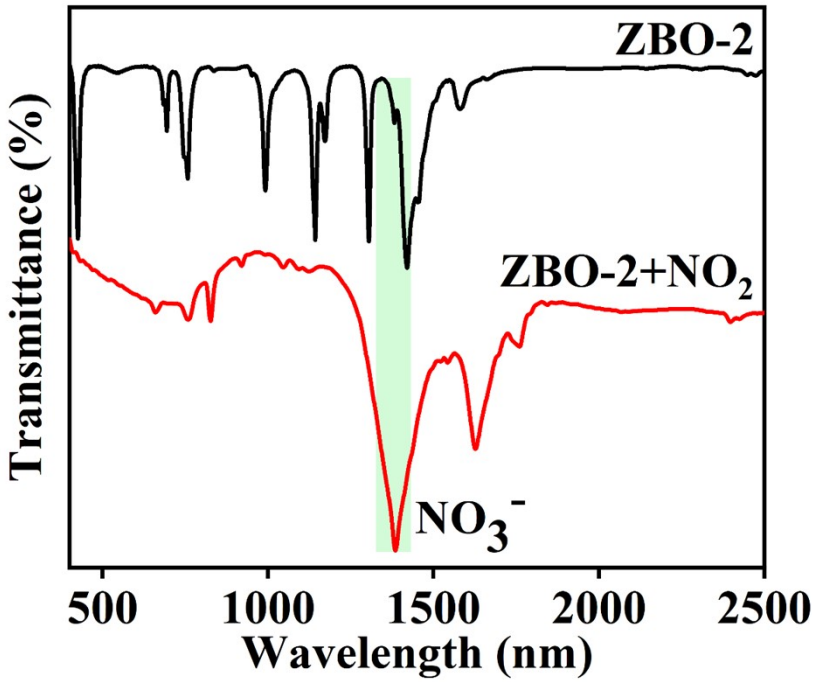

Fig. S10 FT-IR spectra for ZBO-2 composite in air and exposed to NO_2 at RT.

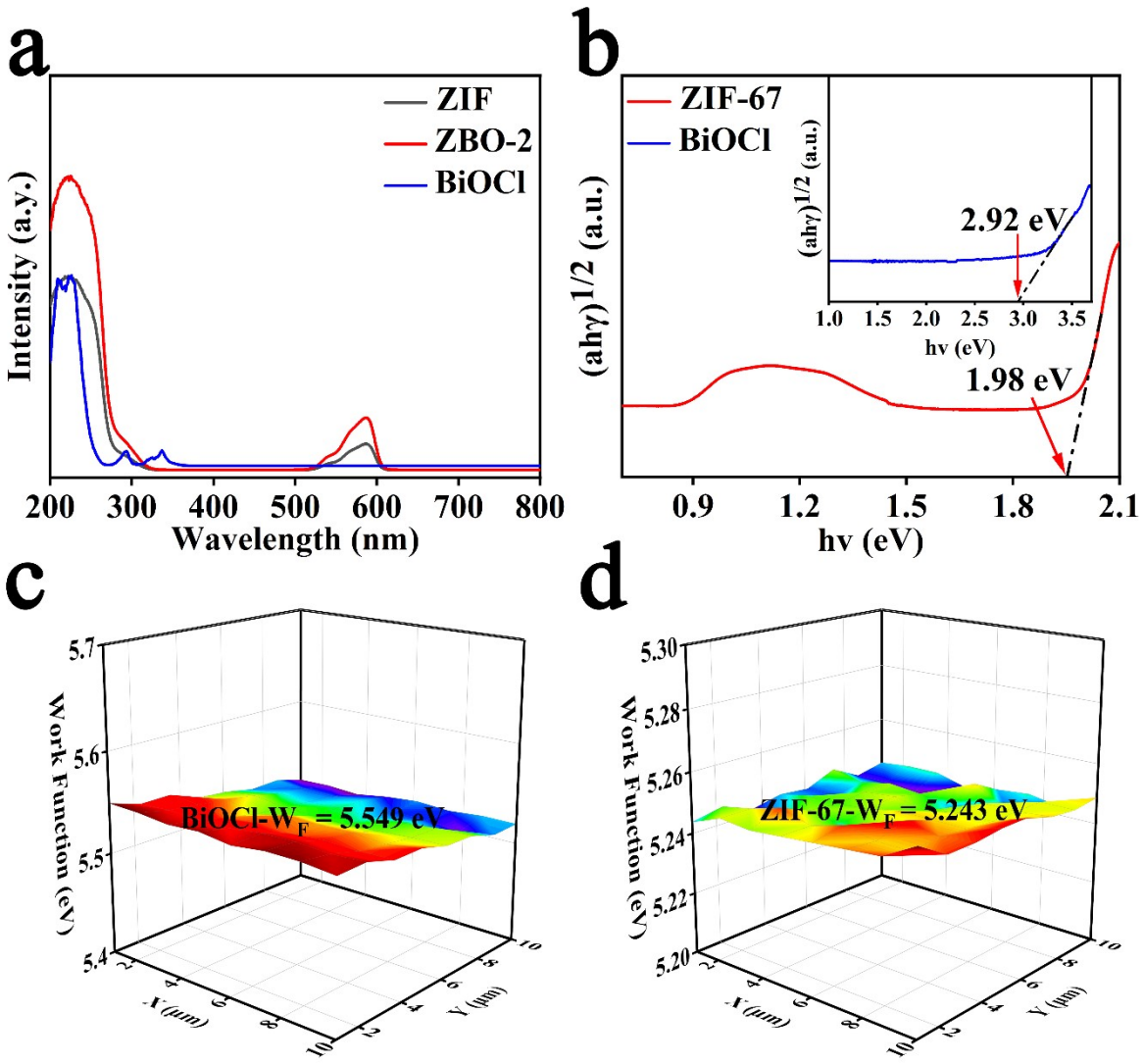

Fig. S11 (a and b) Uv-vis diffuse reflectance spectra of BiOCl, ZIF-67, and ZBO-2 (the energy value at the intersection of tangent and the horizontal axis is the optical band gap); (c and d) Kelvin probe scheme for pure ZIF-67 and BiOCl NSs.

References

1. Ullah, M.; Bai, X.; Chen, J.; Lv, H.; Liu, Z.; Zhang, Y.; Wang, J.; Sun, B.; Li, L.; Shi, K., Metal-organic framework material derived Co_3O_4 coupled with graphitic carbon nitride as highly sensitive NO_2 gas sensor at room temperature. *Colloids and Surfaces A: Physicochemical and Engineering Aspects* **2021,** *612*, 125972.
2. Zhan, M.; Ge, C.; Hussain, S.; Alkorbi, A. S.; Alsaiari, R.; Alhemiary, N. A.; Qiao, G.; Liu, G., Enhanced NO_2 gas-sensing performance by core-shell SnO_2/ZIF-8 nanospheres. *Chemosphere* **2022,** *291*, 132842.
3. Liu, Y.; Wang, R.; Zhang, T.; Liu, S.; Fei, T., Zeolitic imidazolate framework-8 (ZIF-8)-coated In_2O_3 nanofibers as an efficient sensing material for ppb-level NO_2 detection. *J Colloid Interface Sci* **2019,** *541*, 249-257.
4. Michel, C. R.; López Contreras, N. L.; Martínez-Preciado, A. H., CO_2 and CO gas sensing properties of nanostructured BiOCl ribbons doped with gold nanoparticles. *Sensors and Actuators B: Chemical* **2012,** *173*, 100-105.
5. Michel, C. R.; Contreras, N. L. L.; Martínez-Preciado, A. H., Gas sensing properties of nanostructured bismuth oxychloride. *Sensors and Actuators B: Chemical* **2011,** *160*, 271-277.
6. Navale, S. T.; Yang, Z.; Liu, C.; Kumar, A.; Sharma, G.; Cao, P.; Patil, V. B.; Stadler, F. J., Solid-state synthesis strategy of hierarchically-structured BiOCl desert-roses for the selective detection of C_2H_5OH. *Journal of Alloys and Compounds* **2019,** *778*, 532-541.
7. Oum, W.; Mirzaei, A.; Hussain, T.; Bang, J. H.; Han, S.; Shin, K. Y.; Yu, D. J.; Kang, S.; Kaewmaraya, T.; Kim, S. S.; Kim, H. W., Room temperature NO_2 sensing performance of a-C-decorated TeO2 nanowires. *Sensors and Actuators B: Chemical* **2022,** 363, 131853.
8. Pasupuleti, K. S.; Reddeppa, M.; Chougule, S. S.; Bak, N. H.; Nam, D. J.; Jung, N.; Cho, H. D.; Kim, S. G.; Kim, M. D., High performance langasite based SAW NO_2 gas sensor using 2D g-C_3N_4@TiO_2 hybrid nanocomposite. *J Hazard Mater* **2022,** *427*, 128174.
9. Tyagi, S.; Kumar, A.; Kumar, A.; Gautam, Y. K.; Kumar, V.; Kumar, Y.; Singh, B. P., Enhancement in the sensitivity and selectivity of Cu functionalized MoS_2 nanoworm thin films for nitrogen dioxide gas sensor. *Materials Research Bulletin* **2022,** 150, 111784.
10. Han, D.; Han, X.; Liu, L.; Li, D.; Liu, Y.; Liu, Z.; Liu, D.; Chen, Y.; Zhuo, K.; Sang, S., Sub-

ppb-Level Detection of Nitrogen Dioxide Based on High-Quality Black Phosphorus. *ACS Appl Mater Interfaces* **2022,** *14*, 13942-13951.

11. Ni, M.; Han, S.; Liang, Z.; Liu, S.; Zhang, X.; Hussain, S.; Wang, M.; Qiao, G.; Liu, G., Enhanced room-temperature NO_2 sensing performance of mulberry-like Cu_2O/CuO composites. *Sensors and Actuators A: Physical* 2023, 350, 114136.
12. Liang, Z.; Zhang, X.; Yang, J.; Cheng, Y.; Hou, H.; Hussain, S.; Liu, J.; Qiao, G.; Liu, G., Facile fabrication of nanoflower-like WO_3/WS_2 heterojunction for highly sensitive NO_2 detection at room temperature. *J Hazard Mater* 2023, 443 (, 130316.
13. Usov, P. M.; McDonnell-Worth, C.; Zhou, F.; MacFarlane, D. R.; D'Alessandro, D. M., The Electrochemical Transformation of the Zeolitic Imidazolate Framework ZIF-67 in Aqueous Electrolytes. *Electrochimica Acta* **2015,** *153*, 433-438.
14. Dua, V.; Surwade, S. P.; Ammu, S.; Agnihotra, S. R.; Jain, S.; Roberts, K. E.; Park, S.; Ruoff, R. S.; Manohar, S. K., All-organic vapor sensor using inkjet-printed reduced graphene oxide. *Angew Chem Int Ed Engl* **2010,** 49, 2154-7.
15. Gu, W.; Yang, L.; Teng, F.; Abiden, Z. U.; Zhao, F., Investigation on Different Electrochemical Behaviors of Four-Layered Bismuth Oxyhalogens. *Energy Technology* **2019,** 7, 1900460.
16. Li, M.; Zhou, D.; Zhao, J.; Zheng, Z.; He, J.; Hu, L.; Xia, Z.; Tang, J.; Liu, H., Resistive gas sensors based on colloidal quantum dot (CQD) solids for hydrogen sulfide detection. *Sensors and Actuators B: Chemical* **2015,** *217*, 198-201.